Performance of the Light Trigger System in the Liquid Xenon γ-Ray Imaging Telescope LXeGRIT

Uwe Oberlack, Elena Aprile, Alessandro Curioni, and Karl-Ludwig Giboni

Abstract—**LXeGRIT is a balloon-borne Compton telescope for MeV γ-ray astrophysics, based on a liquid xenon time projection chamber with charge and light readout. The energy and direction of an incident γ-ray are reconstructed from the three-dimensional locations and energy deposits of individual interactions taking place in the homogeneous detector volume. While the charge signals provide energy information and X–Y-positions, the fast xenon scintillation light signal is used to trigger the detector. The drift time measurement, referred to the time of the trigger signal, gives the Z-position with the known drift velocity. The light is detected by four ultraviolet-sensitive photomultiplier tubes (PMTs). The logical OR of the PMT signals triggers the data-acquisition system with an efficiency that depends on the event energy and location, as well as on the discriminator thresholds used on the individual PMTs. Results from experiments with a tagged ^{22}Na source give the spatial distribution of the light trigger efficiency for 511-keV γ-rays. When averaged over the whole sensitive volume and all PMTs, the trigger efficiency is 47% or 40% for two discriminator windows used during the LXeGRIT balloon flight of 1999. These values are strongly affected by the different sensitivity of each PMT. The corresponding average efficiency at 511 keV for the best of the four PMTs is in fact 63% and approaches 100% for interactions taking place in a small volume right above the PMT.**

Index Terms—**Compton telescope, γ-rays, liquid xenon, scintillation, time projection chamber (TPC), trigger.**

I. INTRODUCTION

GAMMA-RAYS in the MeV energy band have a great scientific potential for astrophysics. They directly address topics as diverse as nucleosynthesis, supernova mechanisms, star formation, and distribution of massive stars or the physics of accreting black holes [1]. Yet, imaging of cosmic MeV γ-rays is notoriously difficult due to the lack of focusing optics, a broad minimum in the cross section of photons with matter, and small source fluxes. This results in the requirement of large-volume massive detectors and long observing times. The situation is further complicated by the atmosphere's opaqueness for γ-rays, requiring telescopes to be put into space or near-space where intense radiation fields generate high background levels and thus signal-to-background ratios of typically 1:100 or less. To meet the demanding sensitivity requirements of current astrophysical questions, new detectors are needed that combine high efficiency, great background
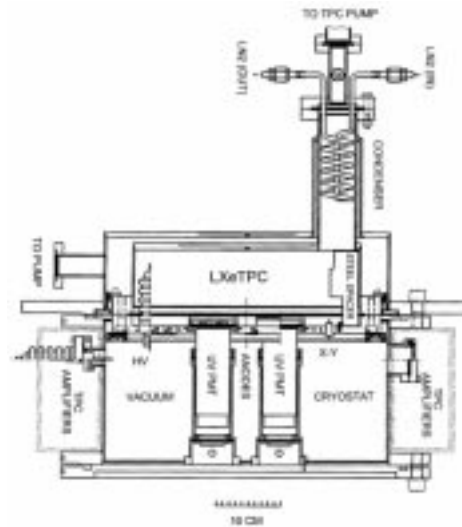
Fig. 1. Mechanical design of the LXeTPC.

suppression capabilities, and a large field-of-view. A Compton telescope is considered the most promising instrument design for MeV γ-ray astrophysics, following the pioneering achievements of the first and only Compton telescope in space to-date, CGRO/COMPTEL [2].

LXeGRIT is a new type of Compton telescope in which γ-rays are imaged in a liquid xenon time projection chamber (LXeTPC), which combines charge and light readout for three-dimensional localization and energy measurement in one homogeneous volume. A simplified mechanical drawing of the LXeGRIT detector is shown in Fig. 1. The TPC structure, with a sensitive area of 20×20 cm^2, is shown in the photograph of Fig. 2, where the cathode plate has been removed to expose the assembly of grid, X–Y wires, anodes, and the windows, through which each photomultiplier tube (PMT) views the detector volume. The drift region between cathode and grid spans 7 cm. Below, separated by 3 mm each, are two arrays of orthogonal wires (62-X and 62-Y) with a pitch of 3 mm and four anodes, made of wire meshes in a metal frame. The ionization electron clouds, produced by γ-ray interactions in the liquid, are drifted in an electric field of 1 kV/cm, kept homogeneous by a series of shaping rings (also visible in Fig. 2). After passing the grid, the drifting charges induce signals on the wires, providing the two-dimensional localization of an interaction. The depth of the interaction (Z-position) is inferred from the drift time measurement, referred to the event time zero provided by the scintillation signal, also produced in an interaction. The energy deposited in each interaction is measured from the collected charge signal(s) on one of the four

anodes. The induction and collection signals are digitized by flash analog-to-digital converters (FADCs) with a sampling rate of 5 MHz and a resolution of 8 and 10 bits, respectively [3].

The TPC structure is mounted on four ceramic rods, screwed on the 16-in stainless steel flange, on which high voltage (HV) and signal feedtroughs are welded along with four quartz windows, one under each of the anode meshes, to allow light transmission to the PMTs. The flange closes the detector in a cylindrical vessel, filled with about 8 l of high-purity liquid xenon. A vacuum cryostat provides the thermal insulation. The liquid temperature is maintained at $\sim -95°$C within a few degrees by controlling the vapor pressure with a flow of liquid nitrogen through a condenser. The detector, originally developed as a laboratory prototype to test the feasibility of a large-volume LXeTPC and to demonstrate its performance with γ-rays, was later converted to a balloon payload for observations of cosmic γ-ray sources. The first balloon flight of LXeGRIT, in 1997, proved the reliable operation of the TPC in near-space environment, validating the design of various critical mechanical, electrical, and cryogenics systems. Shortcomings associated with the data-acquisition system (DAQ) and the trigger electronics, identified during this flight, have been resolved with the development of a new trigger processing unit and a new DAQ processor and software [4]. LXeGRIT, with the upgraded systems, performed successfully during two long balloon flights in 1999 and 2000. A description of the payload in its 1999 flight configuration and results from calibration and flight data are given in [5] and [6].

II. THE LXeGRIT LIGHT TRIGGER SYSTEM

Liquid xenon is an excellent scintillator with a high photon yield similar to that of NaI(Tl) but with a much shorter decay time, consisting of a fast (<5 ns) and a slow (27 ns) component [7], [8]. The scintillation emission peaks in the ultraviolet (UV) at 175 nm. In the LXeGRIT TPC, the scintillation light is detected by four 2-in UV-sensitive PMTs (Electron Tubes 9813QA), coupled to the liquid vessel through four quartz windows 2-in in diameter. Two of the windows, mounted on the detector's flange, are visible in Fig. 2. The distance between each window and the corresponding anode is ~ 3 cm. This is due partially to the metal brace around the window and to the requirement for connecting the four anode signals to a feedthrough in the center of the detector flange. The PMTs are mounted in the vacuum cryostat, as shown in Fig. 1, at a few millimeters from the windows. The typical quantum efficiency of the PMT photocathode is about 15%.

Interactions in the insensitive liquid xenon volume, especially in the layer between PMT windows and anodes, produce a light signal without a charge signal and thus contribute background triggers. The shadowing effect of the metal brace around each window, however, is such that a large fraction of this volume is invisible to the PMTs. The fraction of background triggers depends on the spatial distribution of γ-ray interactions in the chamber and on the trigger settings, which determine the ratio of the trigger efficiency in the dead volume to the average over the sensitive volume. We estimate the contamination with light triggers from the dead volume to 10–30%, and an additional
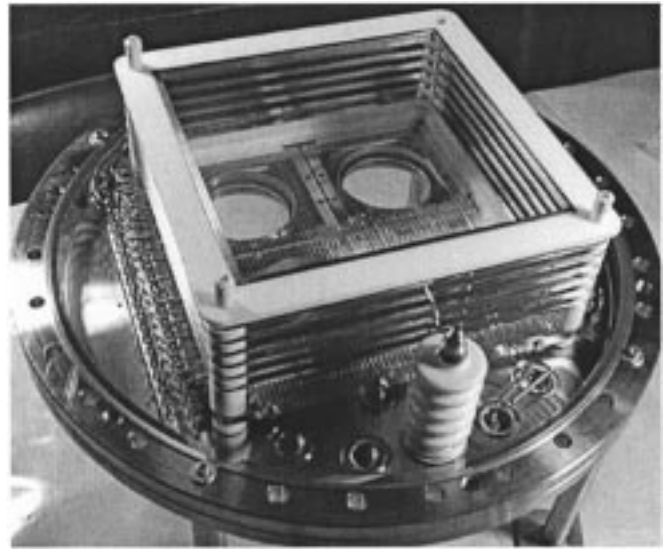

Fig. 2. A photo of the assembled TPC structure taken with the cathode removed to show the readout structure and the windows through which the PMTs view the liquid xenon.
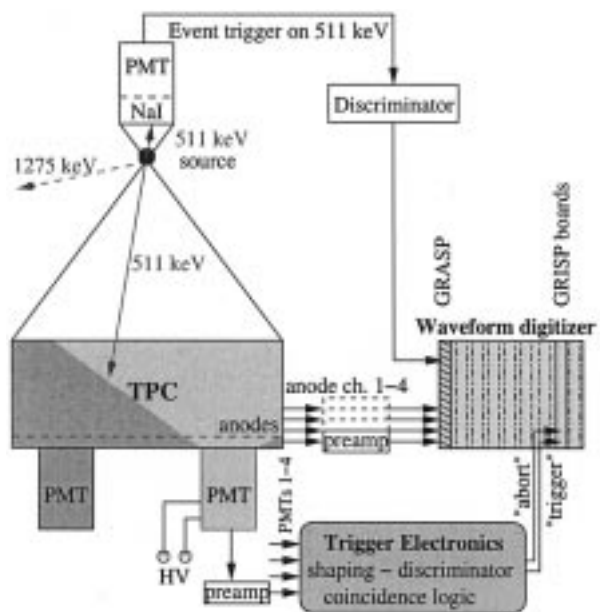

Fig. 3. Setup of the spatially resolved trigger efficiency measurement using the LXeGRIT flight electronics and a tagged ^{22}Na source.

$\sim 10\%$ for interactions within the collection region. An online test for a minimum charge deposit on the anodes keeps triggers from the dead volume from being recorded as events.

While the entire sensitive volume is visible to the PMTs, this TPC design is not optimal for light collection. Since the cathode and the field shaping rings around the drift region have little reflectivity in the UV, solid angle effects are expected to be significant. The W-value for scintillation light in liquid xenon is similar to that for charge, resulting in a large photon yield, i.e., $\sim 6 \cdot 10^4$ photons are generated by a γ-interaction of 1 MeV. However, the number of photons that reach a PMT is drastically reduced by several factors. The largest loss is due to the small solid angle of each PMT for most interaction locations. This results in a typical reduction factor of ~ 0.02, varying widely across the

chamber. Further losses include quenching of the recombination scintillation by the electric field (on the order of 0.5), optical transmission of the grid, X–Y wires, anode mesh, losses at the LXe/quartz interface, optical transmission of the quartz window, and reflection at the PMT window. The resulting number of photons is too small for good energy resolution. The light signal is dominated by solid angle effects, yet it is sufficient to trigger the TPC down to γ-ray energies as low as 100 keV. For the 1997 and 1999 balloon flights, the PMTs were operated at negative HV. To minimize noise from capacitive coupling to the input of the highly sensitive (LXeTPC) anode preamplifiers, positive HV was used instead for the 2000 flight. The PMT signals are processed by charge-sensitive preamplifiers (Clear Pulse Model 5016 Dual CSA) and fed into a custom-made trigger electronics unit (Clear Pulse Model 8823A), where the signals are discriminated and logically combined. The low threshold of a discriminator window is used to suppress noise pulses and to select a minimum signal amplitude. The high threshold can be selected to ignore high-energy signals from cosmic rays. The trigger signal, derived from the logical OR of the four PMTs, can be vetoed by a coincidence signal of plastic and NaI scintillators, used to shield the TPC during the 1997 and 1999 flights. For the 2000 flight, all shields were removed, including the plastic counter. For any PMT signal above the low discriminator threshold, the trigger logic also checks whether a trigger signal was generated within the previous 50 μs, in which case it issues an abort signal to reset the data-acquisition system. The rates after each step in the logic are counted by a 16-channel scaler unit (Clear Pulse Model 8823B) and read by the data-acquisition processor via a VME interface. For further details on the LXeGRIT trigger system and data-acquisition system, we refer to [4].

III. SETUP FOR THE TRIGGER EFFICIENCY MEASUREMENT

The trigger efficiency of the LXeGRIT instrument was measured in a dedicated experiment with a tagged ^{22}Na source. The HV on the four PMTs of the light readout, and the discriminator low and high thresholds, were the same as during the 1999 flight, namely, -1870 , -1800, -1850, and -1870 on PMTs 1–4, respectively. Most of the flight data were taken with the same discriminator window on all four PMTs of 10–128, referred to as setting A in the following, where one unit corresponds to about 10 mV and the scale ranges from 0 to 255. We will refer to a wider discriminator window of 10–255 as setting B. The TPC three-dimensional imaging capability provides the unique opportunity to determine not only the overall trigger efficiency but also its spatial distribution within the sensitive volume. The trigger efficiency as a function of the energy deposited in each volume element can be directly applied to Monte Carlo simulations, in the broader context of representing the overall instrument response.

The FADC readout of the charge signals on wires and anodes provides the energy deposit and the location of each γ-ray interaction of an event. To initiate the recording of the digital image of the event, an external trigger is required. In the trigger efficiency experiment, one of the two back-to-back 511-keV γ-rays from a ^{22}Na source is detected by an NaI(Tl) counter. This signal triggers the TPC. Fig. 3 shows the experimental
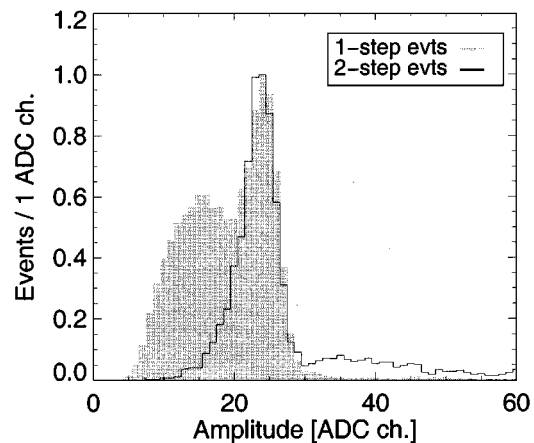

Fig. 4. Normalized ^{22}Na spectra from single and two interaction events measured with the tagged-source setup, for all triggers. The amplitudes were corrected for gain differences among the anodes and for charge loss due to electron attachment.

setup. The ^{22}Na source is centered on the TPC and viewed by an NaI(Tl) counter from the top. The distances between detector and source and between source and counter are adjusted such that for almost each 511-keV photon detected by the NaI(Tl), the other 511-keV photon will hit the TPC, covering the entire sensitive volume. To select annihilation photons with high efficiency, we restrict the NaI(Tl) trigger to the 511-keV photopeak with discriminators. The Xe scintillation signals from the four PMTs were treated with the LXeGRIT trigger electronics. Measurements were made with either one PMT at the time or all four PMTs, connected to the input of the trigger logic unit. The single PMT (HV on the other three PMTs was turned off) was measured to determine the response of the individual PMTs and their contribution to the trigger efficiency, while the measurement with all four PMTs provided the overall efficiency map.

The "trigger" and "abort" signals from the trigger logic unit were fed into two spare channels of the TPC digitizers, so as to record the occurance of a light trigger on an event-by-event basis. The spatially resolved trigger efficiency is derived from the ratio of events with "trigger" signal (and without "abort" signal) divided by all events in the same spatial bin and energy window. In this setup, the trigger efficiency is measured only for energy deposits up to 511 keV.

IV. RESULTS

Fig. 4 shows the ^{22}Na energy spectrum obtained from the digitized anode signals for events recognized with either one interaction (one-step events) or two interactions (two-step events), regardless of a xenon light trigger. The amplitudes have been corrected for gain differences among the four anodes and for charge loss due to electron attachment to electronegative impurities. The electron lifetime is derived from a fit of the exponential decline in photopeak amplitude with drift time, for the sample of one-step events. This results in a best fit value of 332 μs, with a systematic uncertainty of about ± 50 μs. The distribution of one-step events shows a strong Compton tail, largely due to Compton events that scatter backward out of the sensitive
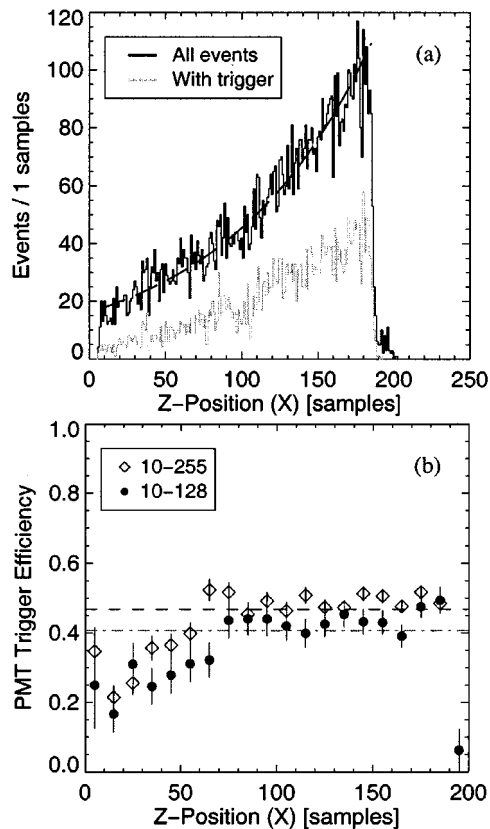
Fig. 5. Z-distributions for 511-keV one-step events with HV and threshold settings as during the 1999 ballon flight and with all four PMTs connected. (a) Z-distribution of all events and of events with a trigger signal. (b) Z-dependence of the overall trigger efficiency, integrated over all X, Y for two discriminator windows (setting A and B).

volume, at high Z (close to the cathode). Very few events show energies beyond the 511-keV photopeak, centered at 24.1 ± 0.2 ADC channels, indicating that the contamination of the sample with background is small. The coincident 1275-keV line does not appear in this spectrum, since, due to the geometry of the setup, almost every event will produce at least one step from a 511-keV photon in the detector. Events from 1275-keV γ-rays would therefore have to show at least two steps. Indeed, the two-step distribution shows significantly more events beyond the 511-keV line. It also shows the effect of Compton tail suppression with multiple interaction events. On-line event selections, such as minimum energy thresholds on wire and anode signals, as well as a minimum and maximum number of wire hits, also affect the shape of the distribution below the annihilation line. In both spectra, the 511-keV line stands out clearly, with similar peak position and width.

Fig. 5 shows the Z-distribution for all 511-keV one-step events, and the corresponding one for events with a light trigger, for setting A (10–128 discriminator window). The distribution is well fitted by an exponential, consistent with the expected attenuation length of about 4 cm for 511-keV γ-rays in LXe. From these data and the corresponding data taken with setting B (10–255), we calculate the light trigger efficiency averaged over all X and Y (thus over all four PMTs) as a function of Z. This is shown on the right panel of the figure for both settings. The efficiency increases with increasing Z, resulting

in average numbers of 40% and 47%, respectively. Several effects influence the Z-distribution of the trigger efficiency.

1) On average over the chamber, the solid angle of each PMT decreases with increasing Z.
2) The area seen by each PMT increases, however, with Z due to the shadowing effect of the metal seal around the window and of the frame that holds the anode mesh.
3) The upper trigger threshold cuts into events predominantly at low Z, where the larger PMT solid angle results in larger light signals.
4) At low Z, reflection losses increase because of the higher index of refraction of quartz compared to the vacuum on top of the PMT photocathode, which leads to total reflection for large incident angles.

The overall trigger efficiency is strongly affected by the different sensitivities of the four PMTs. This is shown in Fig. 6 where the data from the measurement with setting A have been subdivided into the four volumes on top of the individual anodes. The four Z-distributions reflect mainly the response of the individual PMT's, which differ widely in noise levels and therefore sensitivities. PMTs 2 and 3 are most sensitive. Events at high Z still generate triggers with high efficiency despite the reduced solid angle and therefore reduced light signals. At $Z \lesssim 100$ samples (one sample is 0.2 μs or about 0.4 mm), the effect of increasing viewing area dominates, and for setting A, the effect of the upper threshold cut becomes important at low Z. For PMTs 1 and 4, more events are lost below the lower threshold at high Z, which overcompensates the effect of increasing area. For PMT 1, the upper trigger threshold of 128 starts to cut into the distribution at $Z < 40$ samples. This effect is weaker for PMT 4.

Fig. 7 shows the (X, Y)-distribution of the trigger efficiency for 511-keV one-step events for three different Z-slices of the detector volume. The upper three images are for setting A and the lower ones for setting B, with the increased upper discriminator threshold. A slightly different source position for setting B resulted in low statistics at the edges of anodes 1 and 4. The effect of a larger area seen by the PMTs at high Z (especially toward the center of the detector) is apparent. The impact of the upper threshold cut is also clearly seen, especially on PMTs 2 and 3, where the effect extends even to the highest Z-positions. With setting B, the trigger efficiency approaches 100% at low Z in the areas centered on PMTs 2 and 3.

The spatial distribution of the trigger efficiency of individual PMTs is more clearly seen from measurements with a single PMT. For PMT 2 and setting B, results are shown in Fig. 8. The trigger efficiency for 511-keV events within an area of 2-in diameter on top of the PMT, indicated by the dashed circle, is about 75%, averaged over all Z. For setting A, this efficiency drops to ~60%.

Since LXeGRIT requires multiple-step events for Compton imaging, we are interested in the trigger efficiency for this class of events. In principle, this can be fully derived from one-step events, if a complete trigger efficiency map in energy and space were measured, and then applied to Monte Carlo simulations. On the other hand, we can also directly measure the approximate spatial distribution of the trigger efficiency for multiple-step events from the tagged-source experiment,
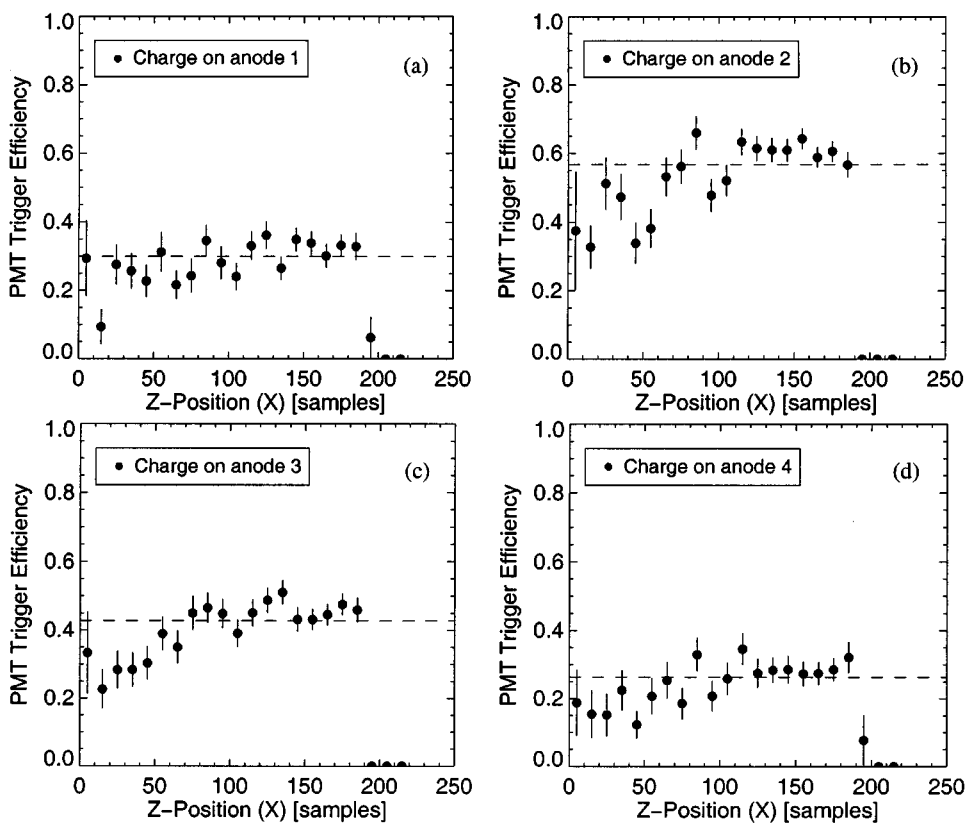
Fig. 6. Z-distributions of the trigger efficiency for 511-keV one-step events, selected by the charge deposit on the individual anodes 1–4 (a)–(d), which mainly reflects triggers on the corresponding PMTs. The discriminator window was 10–128 (setting A).
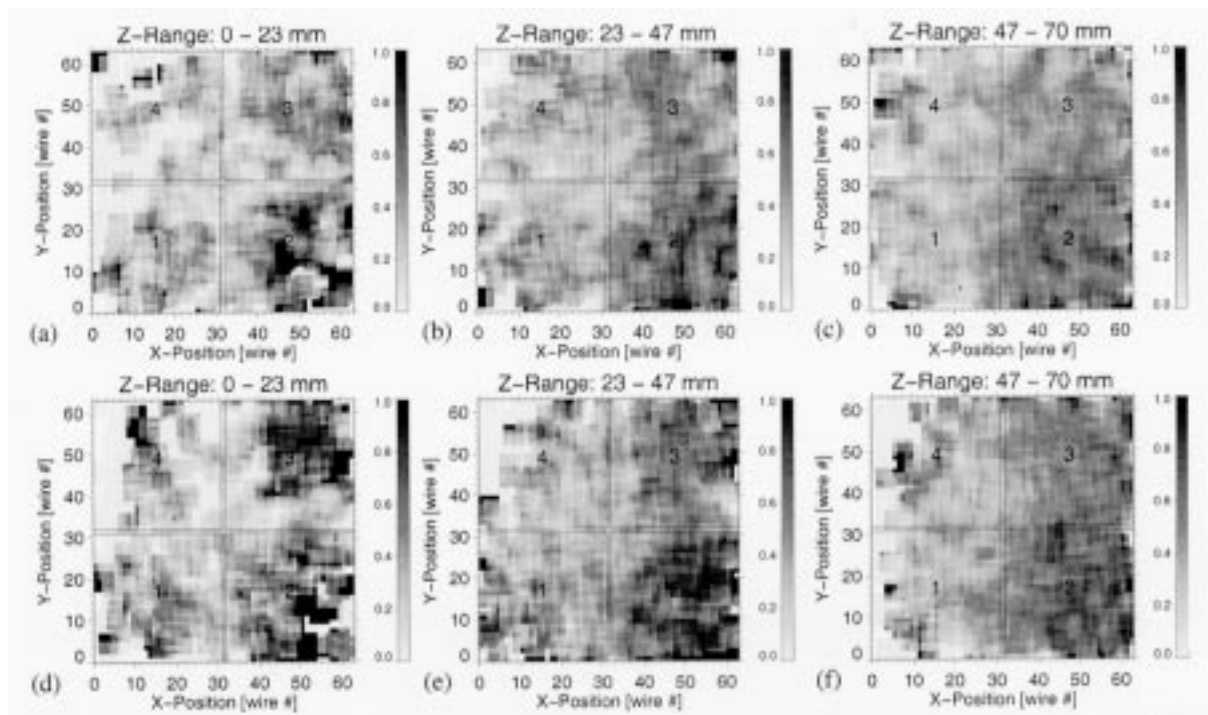

Fig. 7. (X, Y)-distributions of the trigger efficiency for 511-keV one-step events for three different depths of the detector. The four anodes are labeled. (a)–(c) shows data with setting A (10–128), with all four PMTs connected. (d)–(f) shows the corresponding plots with setting B (10–255). The source position for setting B was slightly different from setting A. The images are smoothed over five pixels, and white pixels indicate no data.

even though it is unknown which interaction caused the trigger signal. We studied the spatial distribution for two-step events, calculating the efficiency either by counting each position separately or by weighting the Z-positions by energy deposit.
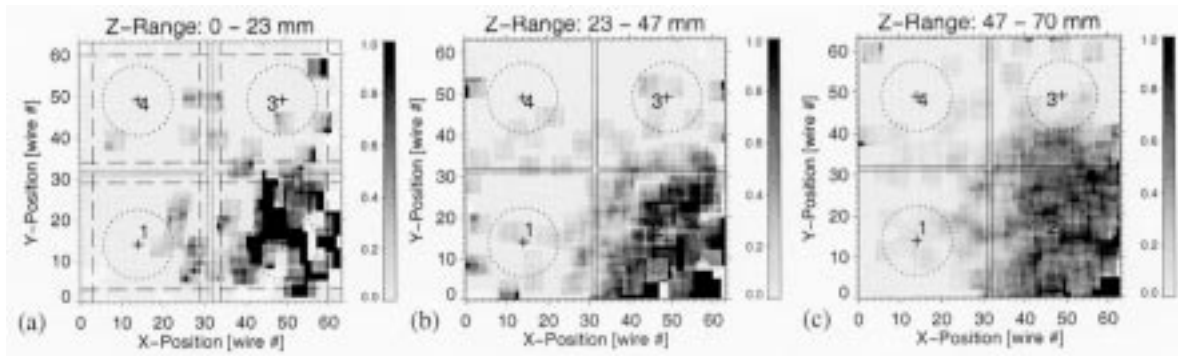
Fig. 8. (X, Y)-distributions of the trigger efficiency as in Fig. 7, but for PMT 2 only and with setting B. In the display of the lower third of the detector (a), dashed lines indicate the anode frame and the 2-in PMTs.
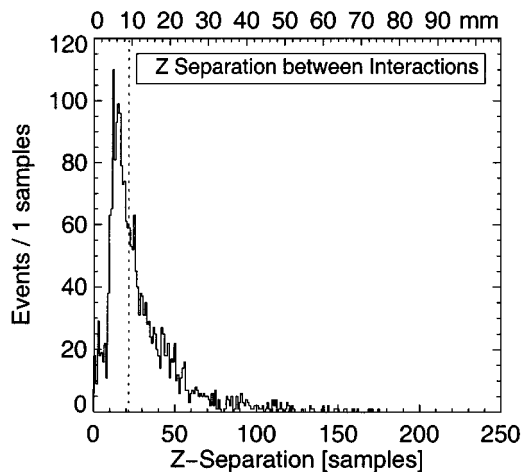

Fig. 9. Z-separation between two steps in the LXeTPC for photons in the 511-keV photopeak. The median of the distribution, indicated by the dashed line, is at about 4 μs (20 samples) drift time, or about 9 mm.

Fig. 10. Z-distribution of the trigger efficiency for two-step events in the LXeTPC for photons in the 511-keV photopeak. We compute the amplitude-weighted average as effective Z-position. The result is very similar to the result for one-step events.

Fig. 9 shows the Z-separation between two interactions for 511-keV γ-rays. The dip in the distribution below about ten samples results from the loss of events due to the inability to fit the amplitude of the two steps on one anode when their Z-separation is so small. Since the median separation in Z is only $\sim$ 9 mm, we expect that the spatial distribution of the trigger efficiency for these events will be similar to that for single interaction events. This is indeed the case, as shown in Fig. 10, for setting A. At higher energies, the spatial separation between interactions becomes larger, and therefore events spread over a larger fraction of the sensitive volume. In this case, the spatial inhomogeneities of the trigger efficiency become less relevant.

Results from these experiments and from the LXeGRIT 1999 balloon flight data [6] have led us to revise the HV and the discriminator thresholds on the PMTs in order to reduce the noise and the trigger sensitivity at low energy. In preparation for the Fall 2000 balloon flight of LXeGRIT, the PMT amplifiers and logic unit were also modified. The combination of lower HV, shorter shaping time, and open discriminator window resulted in a dramatic impact of the instrument trigger response to higher energy photons. This is demonstrated by the energy spectra of an AmBe source from two-step events in Fig. 11. The spectrum to the left was taken with setting A as in 1999 flight configuration. It shows a strong enhancement of low-energy triggers, with the
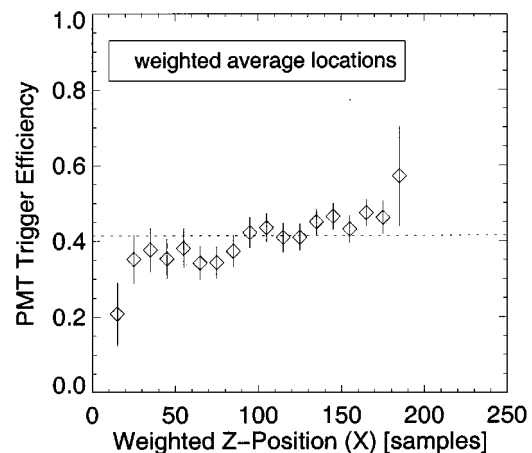
4.43-MeV photopeak largely suppressed. The spectrum to the right was instead derived from a measurement where the PMT's HV was reduced by several hundred volts and the upper discriminator threshold was turned off. The picture is completely changed. The photopeak and the single escape peak are now the dominant features in the spectrum.

V. SUMMARY

We have presented results from experiments dedicated to a spatially resolved measurement of the light trigger efficiency in the LXeGRIT TPC at 511 keV. Data were taken with the HV values and with the two window discriminator thresholds used in the 1999 balloon flight. For the discriminator window 10–128, with which most of the flight data were acquired, the trigger efficiency, averaged over the entire sensitive volume and all four PMTs, was $\sim$40%, and $\sim$47% for the 10–255 window. The large variation in performance of the four PMTs and the higher efficiency value of $\sim$63% on PMT 2 for the 10–255 window indicates that even with the current TPC design, a significantly improved value can be achieved. The trigger efficiency is found to vary widely across the detector due to the different PMT sensitives and to the large variation in solid angle, as well as to other geometrical effects. These variations
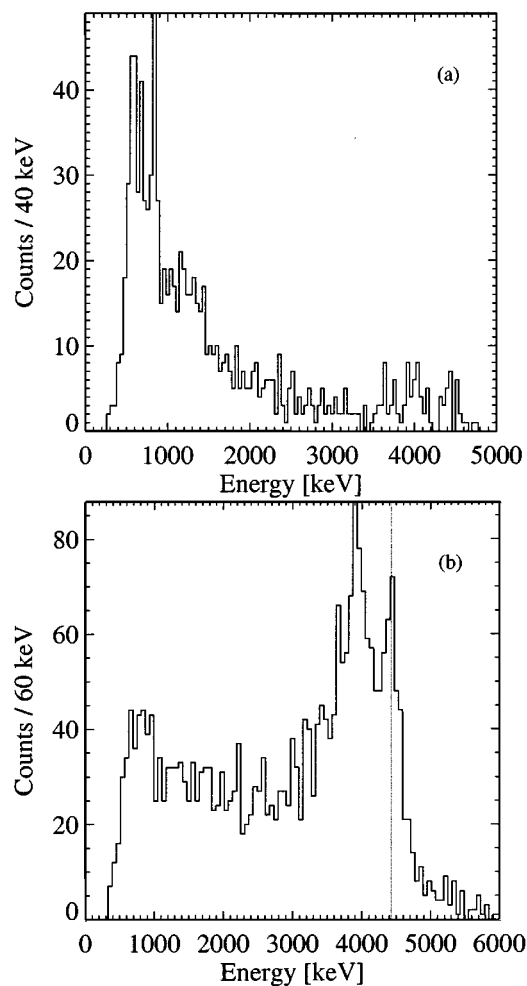
Fig. 11.   AmBe spectra in flight 1999 settings with (a) reduced HV settings and (b) open upper threshold.

and the absence of UV reflectors result in poor light collection efficiency and prohibit the setting of a precise lower energy threshold. This deficiency cannot be solved without significant changes in the chamber itself. For the 2000 flight, we opted

to operate at a lower trigger efficiency in order to reduce the trigger rate from photons below the sensitivity of the charge readout of 150–200 keV.

Additional experiments will extend the three-dimensional trigger efficiency measurement to higher energies. This can be achieved by rotating the ^{22}Na source setup by 90°, again triggering on the 511-keV photopeak. Thus, the second collinear 511-keV photon cannot enter the TPC, while the coincident 1275-keV γ-ray from the deexcitation of ^{22}Ne is emitted isotropically, and can therefore hit the TPC. Other options include triggering on one of two coincident γ-rays (^{60}Co, ^{88}Y) or tagging of β^--radioactive sources with prompt γ-decays (e.g., ^{137}Cs, ^{60}Co) with small plastic scintillation counters to detect the fast electron released in the decay.

REFERENCES

[1] "Recommended priorities for NASA's γ-ray astronomy program 1999–2013," NASA, Goddard Space Flight Center, Greenbelt, MD, NP-1999-04-072-GSFC, 1999.

[2] V. Schönfelder, K. Bennett, J. J. Blom, H. Bloemen, W. Collmar, and A. Connors *et al.*, "The first COMPTEL source catalogue," *Astron. Astrophys. Suppl. Ser.*, vol. 143, pp. 145–179, 2000.

[3] E. Aprile, V. Egorov, K.-L. Giboni, T. Kozu, F. Xu, and T. Doke *et al.*, "The electronics read out and data acquisition system for a liquid xenon time projection chamber as balloon-borne Compton telescope," *Nucl. Instrum. Meth.*, vol. A412, pp. 425–436, 1998.

[4] E. Aprile, A. Curioni, K.-L. Giboni, U. Oberlack, and S. Ventura, "An upgraded data acquisition system for the balloon-borne liquid xenon gamma-ray imaging telescope LXeGRIT," IEEE Trans. Nucl. Sci., 2001, submitted for publication.

[5] E. Aprile, A. Curioni, V. Egorov, K.-L. Giboni, U. G. Oberlack, and S. Ventura *et al..* Spectroscopy and imaging performance of the liquid xenon gamma-ray imaging telescope (LXeGRIT). presented at *Proc. SPIE*. [Online]. Available: http://www.astro.columbia.edu/~lxe/lxegrit

[6] ——, Preliminary results from the 1999 balloon flight of the liquid xenon gamma-ray imaging telescope (LXeGRIT). presented at *Proc. SPIE*. [Online]. Available: http://www.astro.columbia.edu/~lxe/lxegrit

[7] S. Kubota, M. Hishida, M. Suzuki, and J. Ruan, "Dynamical behavior of free electrons in the recombination process in liquid argon, krypton, and xenon," *Phys. Rev. B*, vol. 20, pp. 3486–3496, 1979.

[8] E. Aprile, R. Mukherjee, and M. Suzuki, "A study of the scintillation light induced in liquid xenon by electrons and alpha particles," *IEEE Trans. Nucl. Sci.*, vol. 37, pp. 553–558, 1990.